Postendovascular Aneurysmal Repair Increase in Local Energy Loss for Fusiform Abdominal Aortic Aneurysm: Assessments With 4D flow MRI

Ryota Horiguchi, MD,[1] Yasuo Takehara, MD, DMSc,[1,2*] ⓘ Masataka Sugiyama, MD, PhD,[1]
Ryota Hyodo, MD, PhD,[1] Tomohiro Komada, MD, PhD,[1] Masaya Matsushima, MD, PhD,[1]
Shinji Naganawa, MD, PhD,[1] ⓘ Takashi Mizuno, RT, MSc,[3] Yasuo Sakurai, RT,[3]
Masayuki Sugimoto, MD, PhD,[4] Hiroshi Banno, MD, PhD,[4] Kimihiro Komori, MD, PhD,[4] and
Keiichi Itatani, MD, PhD[5]

Background: Although endovascular aneurysmal repair (EVAR) is a preferred treatment for abdominal aortic aneurysm (AAA) owing to its low invasiveness, its impact on the local hemodynamics has not been fully assessed.
Purpose: To elucidate how EVAR affects the local hemodynamics in terms of energy loss (EL).
Study Type: Prospective single-arm study.
Field Strength/Sequence: A 3.0 T/4D flow MRI using a phase-contrast three-dimensional cine-gradient-echo sequence.
Population: A total of 13 consecutive patients (median [interquartile range] age: 77.0 [73.0, 78.8] years, 11 male) scheduled for EVAR as an initial treatment for fusiform AAA.
Assessment: 4D flow MRI covering the abdominal aorta and bilateral common iliac arteries and the corresponding stent-graft (SG) lumen was performed before and after EVAR. Plasma brain natriuretic peptide (BNP) was measured within 1 week before and 1 month after EVAR. The hemodynamic data, including mean velocity and the local EL, were compared pre-/post-EVAR. EL was correlated with AAA neck angle and with BNP. Patients were subdivided into deformed ($N = 5$) and undeformed SG subgroups ($N = 8$) and pre-/post-EVAR BNP compared in each.
Statistics: Parametric or nonparametric methods. Spearman's rank correlation coefficients (r). The interobserver/ intraobserver variabilities with Bland–Altman plots. A P value < 0.05 is considered significant.
Results: The mean velocity (cm/sec) at the AAA was five times greater after EVAR: 4.79 ± 0.32 vs. 0.91 ± 0.02. The total EL (mW) increased by 1.7 times after EVAR: 0.487 (0.420, 0.706) vs. 0.292 (0.192, 0.420). The total EL was proportional to the AAA neck angle pre-EVAR ($r = 0.691$) and post-EVAR ($r = 0.718$). BNP (pg/mL) was proportional to the total EL post-EVAR ($r = 0.773$). In the deformed SG group, EL (0.349 [0.261, 0.416]) increased 2.4-fold to 0.848 (0.597, 1.13), and the BNP 90.3 (53.6, 105) to 100 (67.2, 123) post-EVAR.
Conclusion: The local EL showed a 1.7-fold increase after EVAR. The larger increase in the EL in the deformed SG group might be a potential concern for frail patients.
Evidence Level: 1
Technical Efficacy: Stage 2

Compared to open surgery, endovascular aneurysmal repair (EVAR) is a preferred treatment, especially for high-risk patients with abdominal aortic aneurysm (AAA) owing to its lower invasiveness.[1–4] Indeed, the perioperative mortality for patients undergoing AAA repair has significantly decreased after the introduction of EVAR.[5] However, EVAR is not necessarily superior to open surgery in the long-term prognosis of patients mainly affected by stent-graft (SG)-related complications[6] such as dislocation or endoleaks.[7,8] In addition to these known limitations, clinicians may not be fully aware of the potential concerns related to the abruptly occurring cardiac burden after EVAR.[9,10] Local energy loss (EL) (mW) refers to the energy dissipation caused by the friction between the viscous fluid and the wall of the flow path as well as the conflicting flow within the fluid.[11,12] By determining the velocity and the coordinate points, the EL is defined using the first spatial differentials of the velocity vector components.[13–16] EL is considered to be an important parameter for estimating the cardiac workload in patients with cardiovascular disorders.[11,17,18] As 4D flow MRI allows three-dimensional (3D) velocimetry in each voxel within the entire field of view (FOV) in a cardiac phase-resolved manner,[19] the EL can be calculated by incorporating the EL equation into flow analysis software[11,15,17] (supplemental text S1). Hence, 4D flow MRI can potentially be used to calculate the local EL of the blood flow in native AAA pre-EVAR and in the implanted SG post-EVAR.

We hypothesized that 1) the EL is high in the AAA due to chaotic intra-aneurysmal hemodynamics,[20] and 2) the correction of the flow path deformities by SG implantation improves the efficiency of blood flow delivery, resulting in a decrease in the local hemodynamic EL after EVAR.

Thus, the aim of our study was to use 4D flow MRI to elucidate how EVAR of AAA affects the acute local hemodynamics in terms of the EL.

Patients and Methods

Study Population

A prospective single-arm study was performed as a part of clinical research approved by the institutional review board of our university hospital. The study was registered with the Japan Registry of Clinical Trials (jRCTs041180157). The minimum target number of patients was estimated as 14 with a statistical software (R-4.2.1 for windows), and written informed consent was obtained from all the enrolled patients.

From April 2019 to April 2020, 14 patients due to undergo elective EVAR as a primary treatment for fusiform AAA were recruited and underwent 4D flow MRI 1–3 days before EVAR and 1–4 days after EVAR. One patient dropped out of the cohort owing to pre-EVAR MR data collection failure (data overflowed from the allotted memory) (Supplemental Fig. S1).

SG Placement

All the patients underwent EVAR for AAA using a SG composed of nitinol frames; eight patients (61.5%) had an Endurant (Medtronic, Minneapolis, MN, USA) stent implanted, while the remaining five patients (38.5%) had an Excluder (Gore Medical, Flagstaff, AZ, USA) stent implanted.

Time-Resolved Contrast-Enhanced 3D MR Angiography

All the patients underwent MR examination using a 3.0 T MR scanner (MAGNETOM Prisma, Siemens Healthineers, Erlangen, Germany) with an 18-channel body matrix coil and 32-channel spine matrix coil.

Before 4D flow MRI, contrast-enhanced (CE) 3D MR angiography (3D MRA) with fast spoiled gradient echo sequence (GRE) was performed after a bolus injection of gadolinium chelate (Gadovist, Bayer Yakuhin, Osaka, Japan) at a dose of 0.1 mmol/kg and an injection rate of 1 mL/sec followed by 20 mL of saline flush with the same injection rate using an autoinjector. The parameters used were as follows: repetition time (TR) (msec)/echo time (TE) (msec)/flip angle (FA) (°)/number of excitations (NEX); 2.95/1.07/19–21/1, FOV (mm); 297 × 340, slice thickness (mm); 2.0–2.4, slice zero-fill interpolation; 50%, matrix; 256 × 224, pixel bandwidth; 650 Hz/Px, acceleration factor; 2, slices per slab; 52, with 17–20 CE dynamic phases.

2D-Cine Phase-Contrast MRI

Before 4D flow MRI, retrospective ECG-gated segmented (factor of 2) 2D-cine phase-contrast (PC) MRI was performed under free breathing using a through-plane velocity encoded GRE at the transverse sections above the abdominal aorta (AA) and the bilateral common iliac arteries (CIAs). The parameters used were as follows: TR (msec)/TE (msec)/FA (°)/NEX; 5.33.11/20/1, FOV (mm); 233 × 340, matrix; 192 × 79, pixel bandwidth; 440 Hz/Px, slice thickness (mm); 6 mm, velocity encoding (VENC) (cm/sec); 200 and cine phases; 23.

The velocimetry for each location was then performed.

4D Flow MRI

The VENC for the 4D flow MRI was determined on the basis of the maximum flow velocity values measured with 2D cine PC MRI, to which a safety margin of 20 cm/sec was added to avoid aliasing.

Coronal 4D flow MRI using a 3D-cine PC GRE covering the abdominal aorta and bilateral CIAs was performed using retrospective ECG gating with the following parameters: TR (msec)/TE (msec)/FA (°)/NEX; 5.4–5.9/2.6–2.9/8/1, FOV (mm); 400 × 294, matrix; 208 × 144, pixel bandwidth 445 Hz/Px, slice thickness (mm); 1–2, slices per slab; 40–60, number of segments; 2, 23 reconstructed phases,

approximate imaging time (min); 7–10, with an acceleration factor of 3 employing generalized autocalibrating partially parallel acquisitions (GRAPPA).

Postprocessing of the 4D Flow MRI Data

The 4D flow MRI and CE 3D MRA data were postprocessed using dedicated flow analysis software (iTFlow ver. 1.9, CardioFlowDesign, Tokyo, Japan). After segmentation of the flow velocity vectors using CE 3D MRA, the intra-arterial flow velocimetry, 3D vector fields, streamline, pathline, and EL maps were generated.

Measurements for AAA Pre- and Post-EVAR

One of the multiple phases that provided the best results in terms of homogeneity and maximum opacification of the aortic lumen was selected from a series of phase-resolved 3D CE MRI (Supplemental Fig.S2). Using iTFlow, the maximum short-axial diameter of the aneurysmal neck (neckD) and the AAA (anD) on the short-axial planes perpendicular to the midline of the aorta or the SG (Supplemental Fig. S3) were measured. For the post-EVAR AA, the maximum aneurysmal neck diameter was measured in the same way as pre-EVAR AA at the same level. The areas including anD and the volumes between neckD and the right and left CIA (RCIA and LCIA) were then automatically calculated by selecting the locations of each anatomical portion using software. Then, the aneurysmal dilatation ratio, that is, anD/neckD was calculated. The neck angle or bent angle (degree) at the neck formed by the midlines of the upstream aorta and the AAA were also measured (Supplemental Fig. S4). All the aforementioned morphological measurements were independently performed by two operators (R. H. with 6 years and Y. T with 37 years of experiences in diagnostic radiology), and the values were averaged.

Interobserver agreement was reported for the measurements of the neck angle.

The patients were subcategorized into "deformed SG" and "nondeformed SG" groups. Patients in the deformed SG group were those with limb narrowing >70% (Supplemental Fig. S5) or neck angle >45°. Analyses were performed for the group as a whole and for the subgroups. Their hemodynamics and brain natriuretic peptide (BNP) values were further assessed separately.

Hemodynamic Assessments for AAA and SG

Flow measurements were performed for the AAA, SG, and bilateral CIAs or bilateral SG limbs pre- and post-EVAR. The measurement planes were placed immediately above the origin of the celiac artery (Ao1), at the AA immediately below the origin of the most caudal major renal artery (Ao2), at the plane with the largest diameter of the AAA (Ao3) and at the midportion of the RCIA and the LCIA. The flow measurement planes were placed perpendicular to the midline of the aorta at Ao1, Ao2, Ao3, RCIA, and LCIA

(Supplemental Fig. S6). For the flow measurement after EVAR, the plane was placed at the same levels as those before EVAR, but perpendicular to each SG. The area-averaged flow velocity and the flow rate values were expressed in cm/sec and mL/sec, respectively. The cardiac phase-resolved and temporally averaged values were measured. In addition, the flow rate values standardized to the values measure at Ao1 were calculated.

The ELs for the blood volume in the luminal segment between Ao1 and Ao2 (neckEL), for the luminal segment of the AAA (anEL; the lumen ranging from Ao2 through the whole common iliac arteries) and for the lumen of the SG (sgEL; the lumen ranging from the upper end of the SG through the end of both limbs in the common iliac arteries) were measured (Fig. 1). The EL measurements were performed on a cardiac phase-resolved basis as well as the integrated basis over the cardiac cycle. We defined (neckEL pre-EVAR) + anEL as "total EL pre-EVAR," and (neckEL post-EVAR) + sgEL as "total EL post-EVAR."

The interobserver and intraobserver agreements were reported for the measurements of EL by two observers.

BNP Test

To assess the cardiac burden of EVAR, the plasma BNP was measured within 1 week before and 1 month after EVAR.

Laboratory Tests

Laboratory tests including total protein, albumin, glucose, estimated glomerular filtration rate (eGFR), potassium, aspartate aminotransferase (AST), alanine aminotransferase (ALT), lactate dehydrogenase (LD), total bilirubin, direct bilirubin, red blood cell count (RBC), and hematocrit (Hct) were performed within 3 days before and after EVAR. The Hct and albumin data were also used to estimate the individual blood viscosity values for the calculation of each EL.[21]

Statistics

The time-resolved EL measurements for each cardiac phase were evaluated with a repeated-measures analysis of variance (ANOVA) followed by the Dunnet test. All the numerical data were expressed as mean ± standard error (SE) when normally distributed or as median and interquartile range otherwise. The differences in the mean values were analyzed using a Student's paired t-test, where the Kolmogorov–Smirnov test determined that data had a normal distribution. Otherwise, the differences of the medians were assessed by a Wilcoxon test. For comparisons between the subdivided groups (deformed SG and nondeformed SG), the Man-Whitney test or Wilcoxon test was used. Regression analysis for correlation was assessed using Spearman's test and expressed with Spearman's coefficient of rank correlation with 95% confident interval. The intra and interobserver variabilities were assessed using Bland–Altman plots.
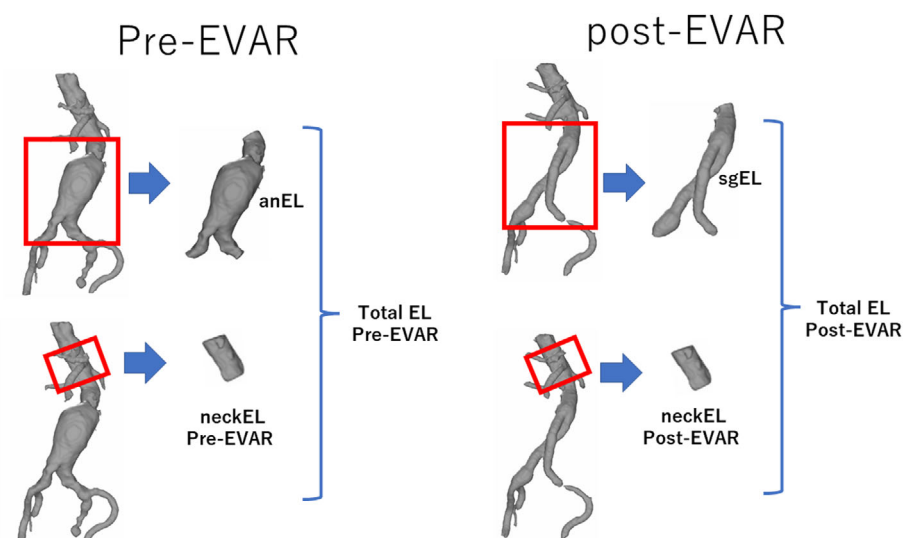
FIGURE 1: Scheme showing the range of the energy loss (EL) measurements (red square) in volume-rendered MR angiography. The EL for the aortic aneurysm (anEL) and the corresponding area for the stent-graft (sgEL) and EL at the aneurysmal neck (neckEL) before and after the endovascular aneurysmal repair (EVAR) are shown. The measurements were performed on a cardiac phase-resolved basis and an integrated basis over the cardiac cycle. We defined (neckEL pre-EVAR) + anEL as total EL pre-EVAR, and (neck-EL post-EVAR) + sgEL as total EL post-EVAR.

A P value of <0.05 was taken as statistically significant. Statistical analyses were performed using StatFlex (Artech, Osaka, Japan) or Medcalc (MedcalcSoftware, Ostend, Belgium).

Results

One patient dropped out from the cohort because data of the pre-EVAR 4D flow MRI overflowed from the allotted

			Pre-EVAR				Post-EVAR			
Patient #	Age (years)	Sex	AAA Volume (cm³)	Neck angle (°)	SG Luminal Volume (cm³)	Background	Neck Angle (°)	Bent Neck >45°	Narrowed SG Limb > 70%	SG Deformity
1	74	M	131	105	110	Angina pectoris	64	+	+(L)	+
2	78	F	196	40	68		39			−
3	81	M	313	96	183		91	+		+
4	73	M	150	30	82		30			−
5	73	M	103	0	65		0			−
6	72	M	122	59	63	Myocardial infarction	45	+	+(L)	+
7	78	M	117	19	56		15			−
8	85	M	434	81	81	Renal dysfunction	57	+	+(R&L)	+
9	78	M	78	52	50		43			−
10	74	M	104	48	53	Diabetes mellitus	26			−
11	84	M	102	39	64	Renal dysfunction	29			−
12	73	M	134	46	59		39		+(L)	+
13	77	F	220	46	91		40			−

TABLE 1. Patient Demographics and Morphological Findings of AAA and SG

AAA = abdominal aortic aneurysm; SG = stent graft; L = left side; R&L = bilateral.

computer memory, and the images could not be reconstructed. Although the initial target number of 14 patients was not fulfilled, 13 patients, 11 male and two female, median age (years) of 77.0 (73.0, 78.8), was secured (Table 1) (Supplemental Fig. S1).

Compatibility of the SG

As confirmed in our preliminary in vitro experiments and in vivo pilot study, the Nitinol stents, namely Endurant and Excluder, produced few artifacts during MRI with the parameters employed in this study.

Our flow phantom study indicated that the nitinol SG-related error in measuring EL was less than 10% of the measured EL in vivo within the aorta or SG (unpublished data).

Morphological Changes Between Pre-EVAR and Post-EVAR

The morphological changes that occurred on the abdominal aortic lumen after EVAR were significant (Table 2). The

dilatation ratio of the AAA was 2.38 ± 0.18. The mean cross-sectional area (cm^2) post-EVAR at Ao3, that is, 2.99 (2.56, 3.27), was significantly smaller than that pre-EVAR, that is, 15.3 (12.2, 24.1). The Ao3/Ao2 area ratio significantly decreased to 0.832 ± 0.0456 post-EVAR compared to 4.71 ± 0.721 pre-EVAR. The volume of the flow path (cm^3) significantly decreased from 131 (103, 202) pre-EVAR to 64.7 (58.4, 84.5) post-EVAR. Although the neck angle (degree) significantly decreased from 50.8 ± 8.12 pre-EVAR to 39.0 ± 6.27 post-EVAR, the neck angle post-EVAR remained proportional to that pre-EVAR ($r = 0.902$ [95% CI: 0.698, 0.971]).

In four cases, either side of the SG limbs or the landing zone of the SG at the iliac artery was narrowed by more than 70%. Moreover, in four cases, the neck angle remained greater than $45°$ after EVAR (Table 1).

Concerning the interoperator correlations and variations between two operators in terms of integrated neck angle measurements, the correlation was significant with

TABLE 2. Morphological and Hemodynamic Assessments Before and After Endovascular Aortic Repair

Characteristics	Pre-EVAR ($n = 13$)	Post-EVAR ($n = 13$)	P
Volume (cm^3)	131 (103, 202)	64.7 (58.4, 84,5)	0.0015
Ao3/Ao2 area ratio	4.71 ± 0.721	0.832 ± 0.0456	0.0001
Neck Angle (°)	50.8 ± 8.12	39.8 ± 6.27	0.0057
Ao1 Flow Rate (mL/sec)	30.3 (27,4, 38.9)	41.0 (37.3, 43.8)	0.0869
Ao2 Flow Rate (mL/sec)	15.9 (11.6, 16.7)	13.3 (11.7, 16.1)	0.249
Standardized	0.495 (0.392, 0.529)	0.353 (0.296, 0.443)	0.116
RCIA Flow Rate (mL/sec)	6.14 ± 0.686	7.43 ± 0.493	0.0326
Standardized	0.188 (0.136, 0.207)	0.180 (0.159, 0.202)	0.463
LCIA Flow Rate (mL/sec)	7.25 ± 0.704	7.58 ± 0.681	0.61
Standardized	0.215 ± 0.0182	0.208 ± 0.0266	0.7
Ao3 velocity (cm/s)	0.910 ± 0.016	4.79 ± 0.32	0.00024
Standardized	0.0253 ± 0.0058	0.119 ± 0.014	0.00024
anEL vs. sgEL (mW)	0.229 (0.132, 0.308)	0.484 (0.418, 0.704)	0.0019
neckEL (mW)	0.0669 (0.0531, 0.0105)	0.113 (0.0724, 0.144)	0.0071
totalEL (mW)	0.292 (0.192, 0.420)	0.487 (0.420, 0.706)	0.0030
Systolic blood pressure (mmHg)	120 (114, 132)	126 (118, 134)	0.972
Diastolic blood pressure (mmHg)	73.8 ± 3.42	66.5 ± 2.35	0.074
Pulse pressure (mmHg)	48.0 (43.0, 65.5)	57.0 (54.3, 64.8)	0.084

Data are median with interquartile range in parentheses or mean ± standard error.
Ao2 = the abdominal aorta right below the origin of the most caudal major renal artery and the corresponding level of the stent graft; Ao3 = the level of the largest cross section of the aneurysm before EVAR and the corresponding level of the stent graft; anEL = aneurysmal energy loss; sgEL = stent graft energy loss; neckEL = aneurysmal neck energy loss; RCIA = right common iliac artery; LCIA = left common iliac artery; standardized = flow rate standardized by Ao1 flow rate (i.e. Ao2/Ao1 or Ao3/Ao1).
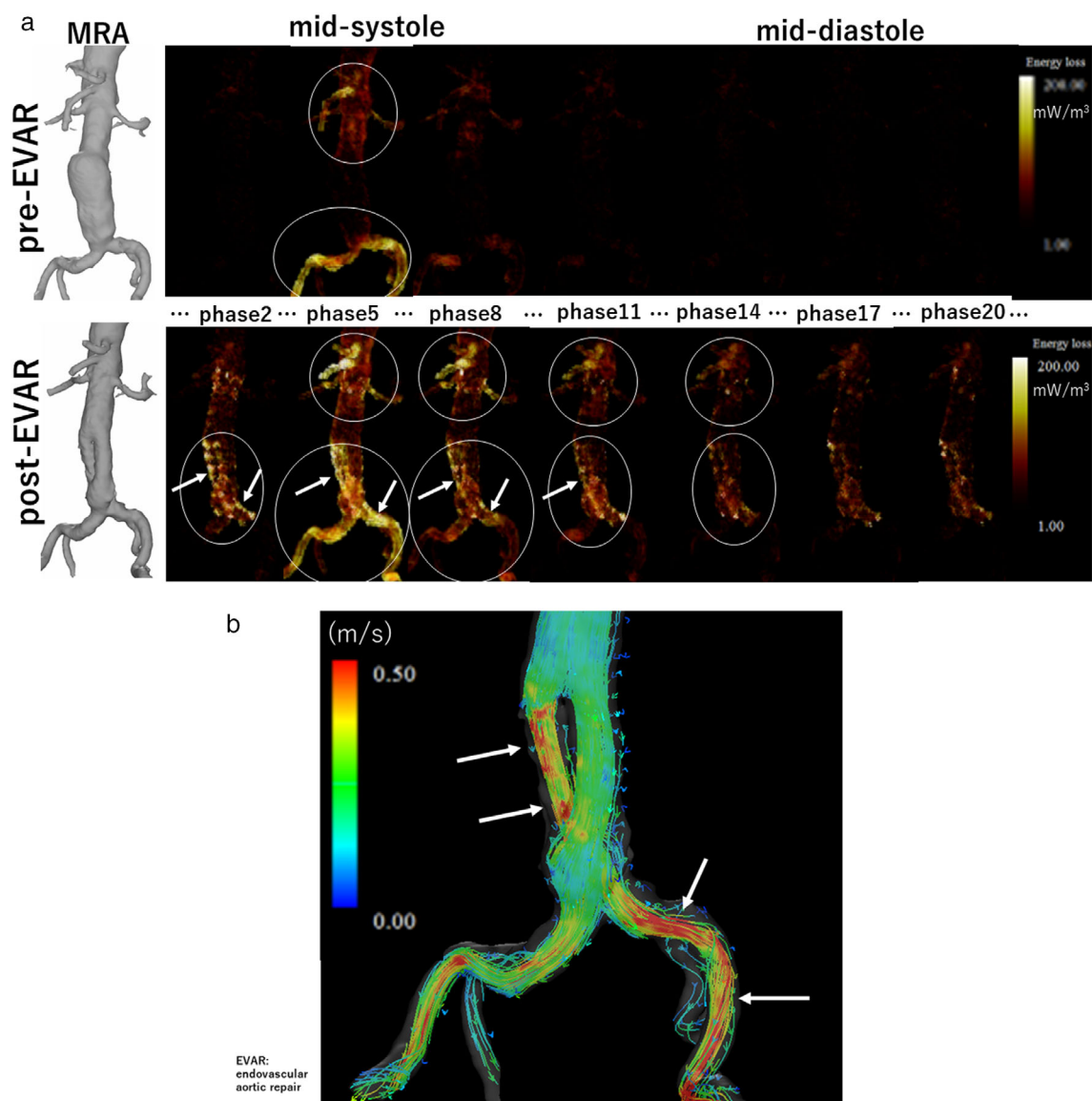
FIGURE 2: (a) Seven representative phases selected from 23 cardiac phase-resolved 3D depictions of the energy loss (EL) map (encoded within the 3D MR angiogram) before (upper row) and after (lower row) stent-graft (SG) placement assessed for a male in his 70s suffering from infrarenal fusiform AAA. Upper row: Before endovascular aortic repair (EVAR), the main energy loss (EL) occurs around the aneurysmal neck and the common iliac arteries at the systole (circles). Lower row: EL measured post-EVAR for corresponding seven phases. Note significantly higher and prolonged EL within the neck and the stent-graft almost at all phases (circles) compared to those of pre-EVAR, particularly at the SG limb with smaller caliber (arrows). (b) The anterior projection of three-dimensional streamline image at the systole for the same patient as that in Fig. 2 after endovascular aortic repair (EVAR). Note that the helical flow of higher velocity (shown red in the streamlines) within the left side of the stent-graft (SG) limb with a smaller caliber (arrows) corresponds to the higher and prolonged energy loss (EL) segment shown in Fig. 2.

$r = 0.898$, and the bias was small with mean differences and upper and lower limit of -2.1 (14.7, -18.8) (Supplemental Fig. S7).

Hemodynamic Changes Between Pre-EVAR and Post-EVAR

Although not statistically significant, the mean flow rate (mL/sec) at Ao1 was higher after EVAR; 30.3 (27.4, 38.9) vs. 41.0 (37.3, 43.8) ($P = 0.0869$) (Table 2). The mean flow velocity (cm/sec) at Ao3 after EVAR (4.79 ± 0.32) was significantly higher (by a factor close to 5) than that before EVAR (0.910 ± 0.016).

The EL was found to increase significantly at the systole and the early diastole (Figs. 2a,b and 3a–c).

The anEL (mW) of 0.229 (0.132, 0.308) measured pre-EVAR significantly increased to the sgEL of 0.484 (0.418, 0.704) post-EVAR (Table 2). Similarly, the neckEL (mW) post-EVAR, that is, 0.113 (0.0724, 0.144) was significantly higher than that pre-EVAR, that is, 0.0669 (0.0531, 0.0105) (Table 2).

Changes of energy loss of the neckEL, anEL and totalEL
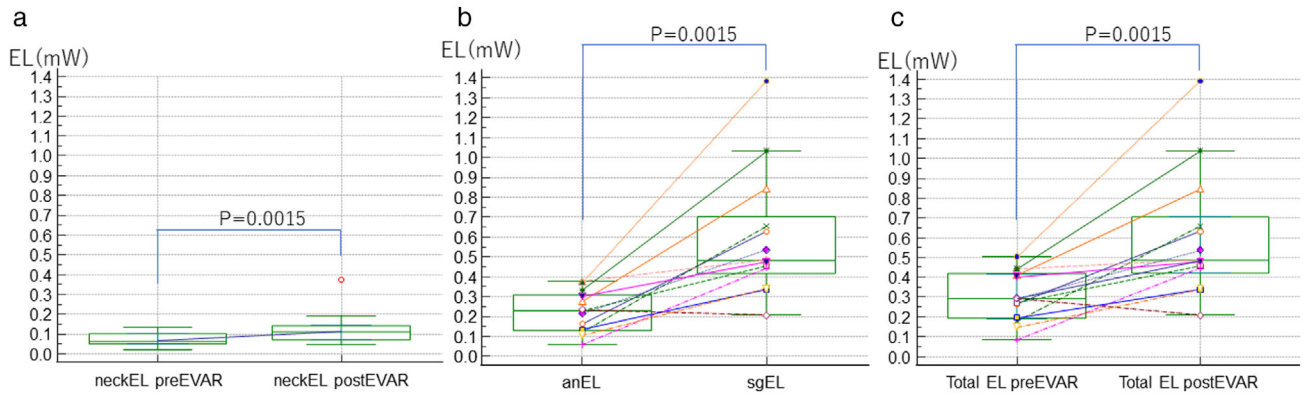between pre- and post-EVAR

FIGURE 3: (a–c) Box-whisker plots comparing energy loss (mW) between pre- and post-EVAR. (a) Note that the neckEL (mW) post-EVAR is higher than that pre-EVAR. (b) The anEL (mW) measured pre-EVAR significantly increased at sgEL post-EVAR. (c) Consequently, the total EL after EVAR was significantly higher than that before EVAR.

Further, anEL was proportional to the AAA volume ($r = 0.687$ [95% CI: 0.219, 0.898], Ao3 area ($r = 0.841$ [95% CI: 0.540, 0.951]) and to the pre-EVAR neck angle ($r = 0.663$ [95% CI: 0.176, 0.889]). After EVAR, sgEL was proportional to the neck angle ($r = 0.718$ [95% CI: 0.276, 0.909]) (Table 3).

There was a correlation between the neckEL pre-EVAR and the neck angle pre-EVAR ($r = 0.715$ [95% CI: 0.271, 0.908]) (Table 3). Similarly, the total EL pre-EVAR was proportional to the neck angle pre-EVAR ($r = 0.691$ [95% CI: 0.225, 0.899]). Likewise, the total EL post-EVAR was proportional to the neck angle post-EVAR ($r = 0.718$ [0.276, 0.909]).

The total EL after EVAR, that is, 0.487 (0.420, 0.706), was significantly higher than that before EVAR, that is, 0.292 (0.192, 0.420) (Fig. 3c) (Table 2).

Laboratory Data

The laboratory data obtained pre- and post-EVAR are summarized in Table 4. Total protein (g/dL) significantly decreased from 7.3 (6.6, 7.7) to 6.4 (6.3, 6.7), albumin (g/dL) significantly decreased from 3.8 (3.6, 4.2) to 3.3 (3.0, 3.4), blood glucose (mg/dL) did not change significantly, that is, 100 (87, 115) vs. 103 (95.0, 117) ($P = 0.382$), eGFR (mL/min/1.73 m^2) significantly increased from 53 (31, 59) to 61 (36, 65), RBC (10^6/μL) significantly decreased from 4.0 (3.5, 4.5) to 3.4 (3.1, 4.0), and Hct (%) significantly decreased from 37 (34, 42) to 33 (30, 37).

Total EL and BNP Values

The plasma BNP values (normal reference ≤ 18.4 pg/mL) were measured 2.5 days (median) before EVAR and 32 days (median) after EVAR. The values (pg/mL) were higher than the normal range both pre-EVAR (74.2 ± 15.2) and post-EVAR (75.8 ± 16.7); however, there was no significant difference between them ($P = 0.946$) (Table 4).

After EVAR, the correlation between the BNP and the total EL was statistically significant with $r = 0.773$ (95% CI: 0.322, 0.938) (Table 3).

The four BNP measurements were missed before EVAR and two measurements were missed after EVAR.

Deformed vs. Nondeformed SG

Five patients had a deformed neck angle of 45° or more and/or narrowing of either SG limb ("deformed SG group") (Table 1). A phase-resolved comparison between the deformed and nondeformed SG groups showed significantly higher EL (Figs. 4a and 5) in the deformed SG group throughout the cardiac cycle except for the early systole. As a result, the patients with a deformed SG showed significantly greater sgEL of 0.883 (0.627, 1.25) than the nondeformed group, that is, 0.495 (0.430, 0.533) (Fig. 6a, b). Similarly, the deformed SG group showed a significantly greater total EL of 0.848 (0.597, 1.13) than the nondeformed SG group, that is, 0.451 (0.340, 0.508) after EVAR (Fig. 6c, d).

In terms of the EL measurements, the intraoperator correlation was $r = 0.995$ (95% CI: 0.991, 0.997) and the interoperator correlation was $r = 0.992$ (95% CI: 0.985, 0.995) (Supplemental Fig. S8a,b). The Bland–Altman plots indicated low intraoperator and interoperator bias with mean differences and upper and lower limit of −0.00171 (0.0431, −0.0465) (Supplemental Fig. S8c,d).

Although the mean BNP values (pg/mL) did not change between pre-EVAR and post-EVAR both were higher than the reference value (Table 4). Although not statistically significant, the median BNP values of the nondeformed SG group decreased from 53.6 (24.6, 106) to 27.4 (14.6, 107) ($P = 0.670$) after EVAR (Fig. 6e). On the other hand, the median BNP of the deformed SG group showed a significant increase to 100 (67.2, 123) after EVAR

TABLE 3. The Relationships Between the Energy Loss and the Anatomical Features, BNP, the Velocity in the Stent-Graft or the Aneurysm, Aneurysmal Neck Measured Pre- and Post-EVAR

		Pre-EVAR			Post-EVAR	
		r (95% CI)	P		r (95% CI)	P
anEL	sgEL					
	dilatation ratio	0.476 (−0.100, 0.814)	0.100	dilatation ratio	N/A	N/A
	volume	0.687 (0.219, 0.898)	0.0095	volume	0.407 (−0.186, 0.782)	0.168
	neck angle	0.663 (0.176, 0.889)	0.00135	neck angle	0.718 (0.276, 0.909)	0.0057
	Ao3 velocity	−0.626 (−0.875, −0.115)	0.0220	Ao3 velocity	0.297 (−0.304, 0.729)	0.325
	Ao3 area	0.841 (0.540, 0.951)	0.0003	Ao3 area	0.0769 (−0.495, 0.602)	0.803
	BNP (pre-EVAR)	0.450 (−0.305, 0.858)	0.224	BNP (post-EVAR)	0.773 (0.322, 0.938)	0.0053
neckEL	neckEL					
	dilatation ratio	−0.0880 (−0.609, 0.487)	0.775	dilatation ratio	N/A	N/A
	volume	0.368 (−0.229, 0.764)	0.216	volume	0.341 (−0.259, 0.751)	0.255
	neck angle	0.715 (0.271, 0.908)	0.0006	neck angle	0.523 (−0.0397, 0.834)	0.0668
	Ao3 velocity	−0.319 (−0.740, 0.282)	0.289	Ao3 velocity	0.357 (−0.241, 0.759)	0.231
	Ao3 area	0.390 (−0.205, 0.775)	0.188	Ao3 area	0.0385 (−0.524, 0.577)	0.901
	BNP (pre-EVAR)	0.333 (−0.425, 0.817)	0.381	BNP (post-EVAR)	0.118 (−0.518, 0.671)	0.729
total EL	total EL					
	dilatation ratio	0.322 (−0.279, 0.741)	0.284	dilatation ratio	N/A	N/A
	volume	0.560 (0.0137, 0.849)	0.0463	volume	0.407 (−0.186, 0.782)	0.168
	neck angle	0.691 (0.225, 0.899)	0.0090	neck angle	0.718 (0.276, 0.909)	0.0057
	Ao3 velocity	−0.538 (−0.840, 0.0178)	0.0576	Ao3 velocity	0.297 (−0.304, 0.729)	0.325
	Ao3 area	0.714 (0.269, 0.908)	0.0061	Ao3 area	0.0769 (−0.495, 0.602)	0.803
	BNP (pre-EVAR)	0.500 (−0.246, 0.874)	0.171	BNP (post-EVAR)	0.733 (0.322, 0.938)	0.0053

anEL = aneurysmal energy loss; sgEL = stent graft energy loss; neckEL = aneurysmal neck energy loss; Ao3 = the level of the largest cross section of the aneurysm before EVAR and the corresponding level of the stent graft.

TABLE 4. Laboratory Data Before and After Endovascular Aortic Repair

Characteristics	Pre-EVAR ($n = 13$)	Post-EVAR ($n = 13$)	P
Total protein (g/dL)	7.3 (6.6, 7.7)	6.4 (6.3, 6.7)	0.0015
Albumin (g/dL)	3.8 (3.6, 4.2)	3.3 (3.0, 3.4)	0.0015
Glucose (mg/dL)	100 (87, 115)	103 (95.0, 117)	0.382
eGFR (mL/min/1.73 m^2)	53 (31, 59)	61 (36, 65)	0.019
K (mEq/L)	4.3 (4.0, 4.8)	4.(3.8, 4.1)	0.0093
AST (IU/L)	19 (16, 23)	19 (16, 28)	0.724
ALT (IU/L)	13 (9.8, 24)	14 (8.8, 19)	0.069
LD (IU/L)	192 (188, 213)	220 (180, 252)	0.162
Total bilirubin (mg/dL)	0.50 (0.48, 0.73)	0.9 (0.75, 1.1)	0.0022
Direct b (mg/dL)	0.1 (0.1, 0.1)	0.1 (0.1, 0.1)	0.306
RBC (10^6/μL)	4.0 (3.5, 4.5)	3.4 (3.1, 4)	0.0088
Hct (%)	37 (34, 42)	33 (30, 37)	0.0071
BNP (pg/mL)	74.2 ± 15.2	75.8 ± 16.7	0.946

Data are median with interquartile range in parentheses.
eGFR = estimated glomerular filtration rate; AST = aspartate aminotransferase; ALT = alanine aminotransferase; LD = lactate dehydrogenase; RBC = red blood cell; Hct = hematcrit; BNP = brain natriuretic peptide.

compared to 90.3 (53.6, 105) before EVAR ($P = 0.0431$) (Fig. 6f).

Discussion

We observed that anEL and total EL pre-EVAR were proportional to the AAA volume and the AAA neck angle. The anEL was inversely proportional to Ao3 velocity, reflecting the reverse pressure gradient occurring in the abruptly dilated AAA, where nonlaminar flows such as a vortex or turbulent flow are dominant.[20] This phenomenon degrades the efficiency of blood flow delivery. Therefore, our initial hypothesis was that the installation of the SG would reduce the EL of the AAA, mainly because it would correct the deformation of the expanded channel and thereby normalize the flow patterns. Previous reports based on computational fluid dynamics (CFD) have indicated that the twisting, bending, and abrupt dilatation observed in the aortic aneurysm impedes the left ventricular outflow.[22,23] Therefore, the cardiac index and stroke volume are affected in such cases. In addition, they subside after aortic aneurysmal repair.[23]

However, contrary to our speculation, the SG placement increased the local EL by a factor of 1.7 in our study. This unexpected result may be primarily due to the highly increased flow velocity within the SG. The SG placement produced significant anatomic and hemodynamic changes in the aorta. First, EVAR reduced the luminal volume by nearly half compared with the pre-EVAR value in our population. As the inflow rate into the SG was slightly increased, the reduced capacity of the SG lumen resulted in an increase in the blood flow velocity in the aortic conduit (at Ao3) by a factor of approximately five.

With regard to the relation with morphological deformities of the SG, sgEL and the total EL were proportional to the neck angle after EVAR. When there is a bend in the aneurysm neck, the aortic conduit becomes narrower. The velocity increases after the narrowed conduit and jet flow occurs in some cases, which promotes the dissipation of kinetic energy, resulting in an overall increase in the local EL. The sgEL of the deformed SG group showed higher and prolonged EL throughout the cardiac cycle compared to that of the nondeformed SG group.

It is intriguing that recent reports on EVAR outcomes have suggested a significant increase in operative mortality in patients with a highly angulated SG neck.[24] The cardiac burden due to the increased EL in a highly angulated SG neck may be a potential risk. We presume that a narrowed SG limb is also a concern for producing jet flow or divergence of the flow, leading to a collision and an increase in the resultant EL in the SG.

In addition to the morphological luminal changes before and after EVAR, other physicomechanical changes must also be considered. In a healthy aorta, the wall has
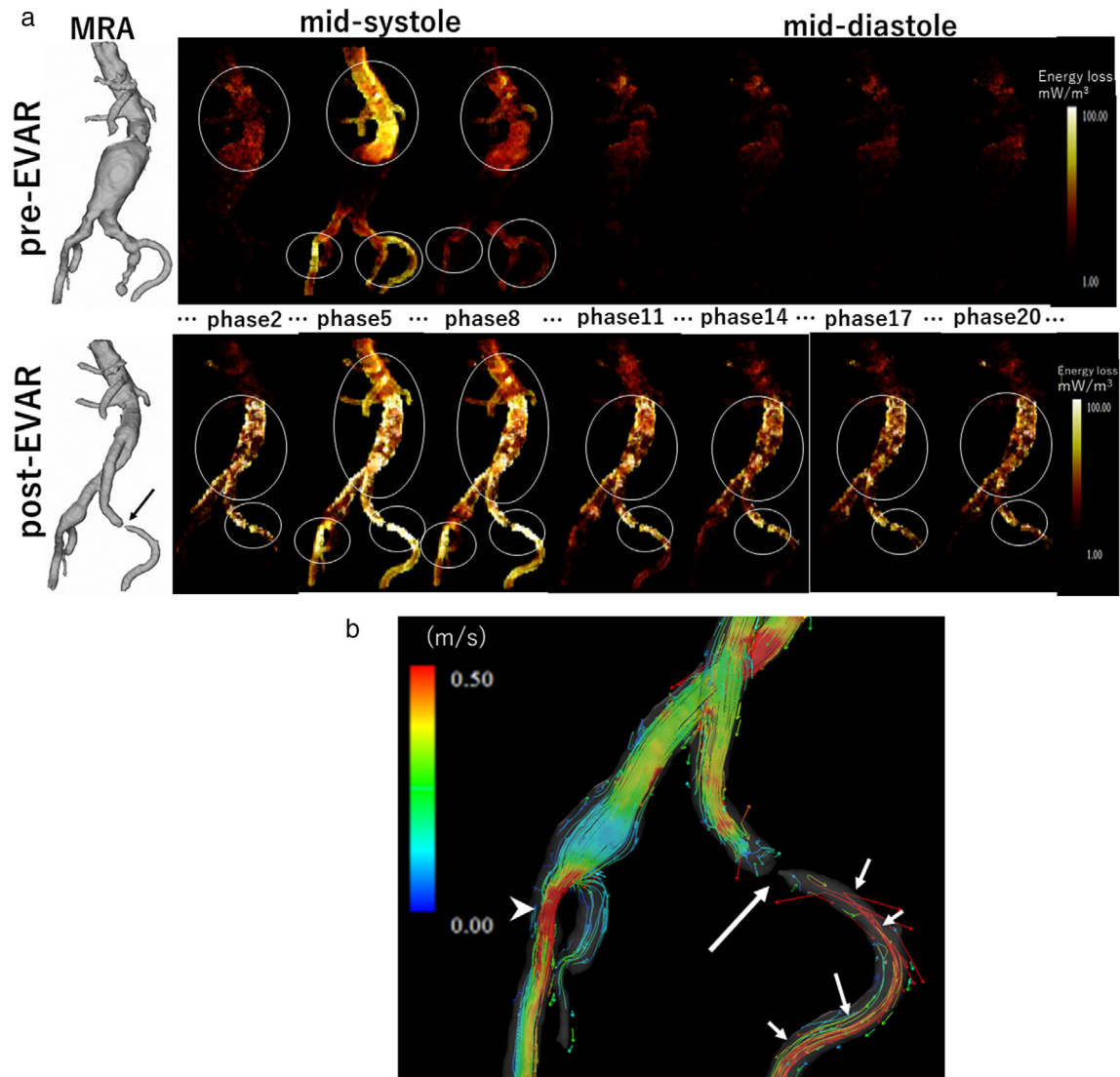
FIGURE 4: (a) Seven representative cardiac phases selected from the 23 phase-resolved energy loss (EL) maps encoded within the contrast-enhanced 3D MR angiography (MRA). Time-resolved depictions of the EL before (upper row) and after endovascular aortic repair (EVAR) (lower row) for a male in his 70s suffering from an infrarenal fusiform aortic aneurysm. This particular patient had a deformed SG (stenotic portion in the left limb). Upper row: Phase-resolved ELs measured pre-EVAR. Note that the main energy loss occurs around the aneurysmal neck and the iliac arteries at a brief period of the systole (circle). Lower row: Seven corresponding phases depicting the energy loss measured post-EVAR. Each phase corresponds to that pre-EVAR shown in the upper row. Note the significantly higher and sustained EL within the SG, including the deformed (stenosed) left limb of the stent-graft (circle) in all phases. (b) Streamline analysis post-EVAR in the same patient as that shown in Fig. 4a. The stenosis was greater than 70% at the left end of the stent graft (SG) (large arrow) where jet flow (small arrow) and fast streamlines are dominant downstream of the stenotic portion. The EL of the right side of the external iliac portion is also high because of a mild but abrupt decrease in the caliber (arrowhead).

optimal elasticity and extensibility, which allows the lumen to expand during the systole to accumulate blood and contract during the diastole to pump the collected blood to the periphery. When the aortic compliance decreases, the pulse wave in an atherosclerotic aorta travels faster than that in a healthy aorta; and then, the reflected pulse wave reaches the heart in the late systole, increasing the cardiac afterload.[25-27] Lower arterial wall compliance also reduces the diastolic pressure, and coronary blood flow,[26] which eventually leads to heart failure.[27,28] Thus, atherosclerosis of the aorta by itself is an independent predictor of future left ventricular (LV) dysfunction.[25-28] SGs are stiffer and less flexible artificial conduits compared to the atherosclerotic aorta. In a dog model experiment, animals with SGs were reported to have more left ventricular hypertrophy than controls.[10] Studies of endovascular aortic repair in humans, mostly thoracic, have reported an increase in the brachial-ankle pulse-wave-velocity and a higher LV-mass-index in the acute and remote phases[9,29] SG implantation reduces the aortic compliance to a greater extent compared to atherosclerosis.[30] Furthermore,
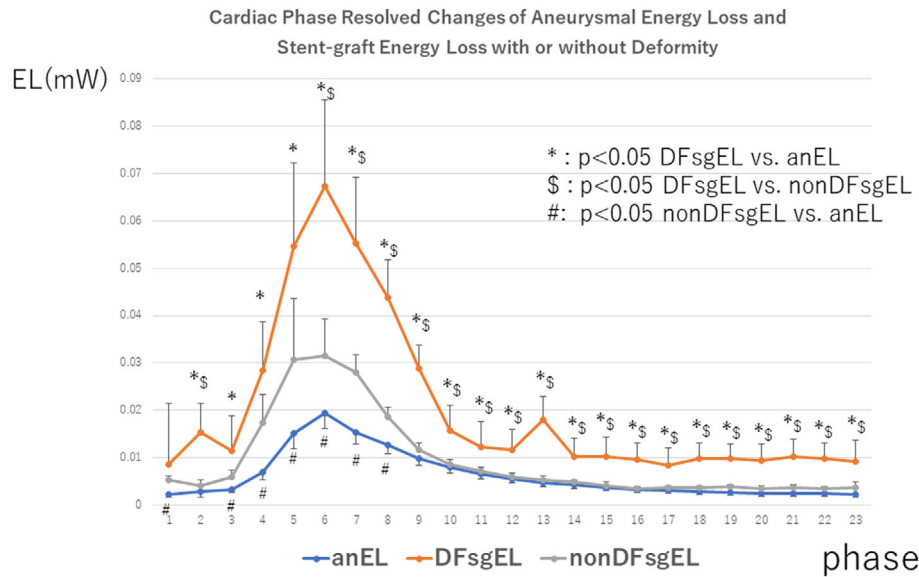
FIGURE 5: Time-resolved comparison of aneurysmal energy loss (anEL) vs. deformed stent-graft EL (DFsgEL) vs. nondeformed sgEL (nonDFsgEL). DFsgEL is always time higher than anEL or nonDFsgEL in any cardiac phase. Non-DFsgEL is higher than anEL at the early systole and the peak systole.
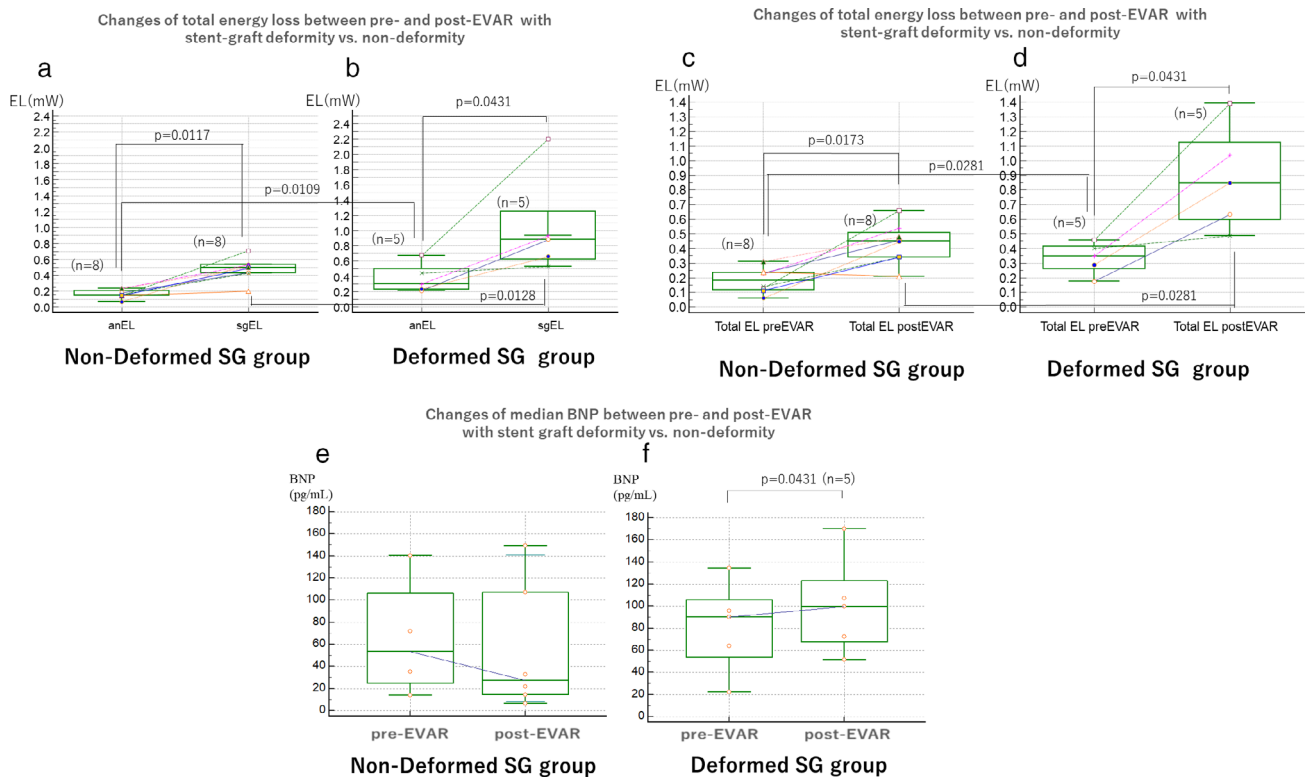

FIGURE 6: (a–f) Changes in the local energy loss (EL) and brain natriuretic peptide (BNP) after endovascular aortic repair (EVAR) between non-deformed and deformed stent-graft (SG). (a, b) Box-whisker plots comparing aneurysmal energy loss (anEL) with sgEL for nondeformed and deformed SG. The EL showed a greater increase for the deformed SG group than for the nondeformed SG group. The patients with a deformed SG showed greater sgEL than the sgEL for the nondeformed group. (c, d) Similarly, the deformed SG group showed a greater total EL than that for the nondeformed SG group after EVAR. (e, f) As for the BNP level, a significant increase in the BNP is observed post-EVAR in the deformed SG group.

atherosclerosis takes decades to develop, and the heart adapts to it, whereas EVAR is an acute event that occurs within a few hours. Considering that the primary aim of an SG is to prevent AAA rupture, EVAR should be an essential therapy, particularly for frail patients who cannot withstand open surgery. However, EVAR increased the local EL in our study,

and the BNP increased significantly in patients with a deformed SG. Plasma BNP levels are known to increase in proportion to the severity of cardiac diseases and have been established as a biochemical marker of heart failure.[31-33] Assuming that the local EL after EVAR is proportional to the plasma BNP level, care should be taken to avoid SG deformities during the procedure. Besides the technical refinement of operators, a more flexible SG that maintains the lumen may be required for future devices.

Limitations

1) Small sample size particularly for subgroup analysis in a single-center study; 2) relatively long interval between BNP measurements and EVAR (median interval of 32 days) as compared to the interval between EVAR and 4D flow MRI after the EVAR (median interval of 1–4 days); 3) BNP measurements missing in 6 of 26 data points (four before EVAR, two after EVAR) owing to insufficient discussion with the attending physician; 4) it should also be noted that the local EL measured using 4D flow MRI is not the overall EL that occurs after EVAR. However, EL after EVAR correlated linearly with the BNP, suggesting that the EL may reflect cardiac burden via factors that are yet to be proven. In the future comprehensive studies involving a larger cohort of patients must be conducted to clarify these factors.

Finally, the possible bias for the increase in the local EL and BNP after EVAR should be discussed. We found that the EL and BNP increased after EVAR, especially in cases involving a deformed SG. Regarding the question as to whether the blood viscosity might increase after EVAR owing to certain factors, the parameters that increase blood viscosity, such as Hct, blood protein, RBC, and glucose concentrations, decreased after EVAR, probably because of the scheduled hydration during admission. Similarly, the BNP has been reported to be inversely correlated with the eGFR[34]; however, in our study, the eGFR increased after EVAR (Table 3), suggesting that possible bias for the increase in the BNP and eGFR after EVAR could not be proven.

Conclusion

The local EL increased by 1.7 times after EVAR. As the local EL after EVAR is proportional to AAA neck angle and plasma BNP, a higher EL with a deformed SG may be a potential concern in frail patients.

Acknowledgments

References

1. Chaikof EL, Dalman RL, Eskandari MK, et al. The Society for Vascular Surgery practice guidelines on the care of patients with an abdominal aortic aneurysm. J Vasc Surg 2018;67(1):2-77 e2.

2. Medical Advisory S. Endovascular repair of abdominal aortic aneurysm: An evidence-based analysis. Ont Health Technol Assess Ser 2002;2(1):1-46.

3. Ulug P, Sweeting MJ, von Allmen RS, Thompson SG, Powell JT, collaborators S. Morphological suitability for endovascular repair, non-intervention rates, and operative mortality in women and men assessed for intact abdominal aortic aneurysm repair: Systematic reviews with meta-analysis. Lancet 2017;389(10088):2482-2491.

4. Wanhainen A, Verzini F, Van Herzeele I, et al. Editor's Choice - European Society for Vascular Surgery (ESVS) 2019 Clinical Practice Guidelines on the Management of Abdominal Aorto-iliac Artery Aneurysms. Eur J Vasc Endovasc Surg 2019;57(1):8-93.

5. Schermerhorn ML, Buck DB, O'Malley AJ, et al. Long-term outcomes of abdominal aortic aneurysm in the Medicare population. N Engl J Med 2015;373(4):328-338.

6. United Kingdom ETI, Greenhalgh RM, Brown LC, et al. Endovascular versus open repair of abdominal aortic aneurysm. N Engl J Med 2010;362(20):1863-1871.

7. Maitrias P, Belhomme D, Molin V, Reix T. Obliterative endoaneurysmorrhaphy with stent graft preservation for treatment of type II progressive endoleak. Eur J Vasc Endovasc Surg 2016;51(1):38-42.

8. Katahashi K, Sano M, Takehara Y, et al. Flow dynamics of type II endoleaks can determine sac expansion after endovascular aneurysm repair using four-dimensional flow-sensitive magnetic resonance imaging analysis. J Vasc Surg 2019;70(1):107-16 e1.

9. Vallerio P, Maloberti A, D'Alessio I, et al. Cardiovascular remodeling after endovascular treatment for thoracic aortic injury. Ann Vasc Surg 2019;61:134-141.

10. Yamashita Y, Oishi Y, Motomatsu Y, et al. Thoracic endografting increases cardiac afterload and leads to left ventricular hypertrophy in dogs. Eur J Cardiothorac Surg 2019;55(4):618-625.

11. Barker AJ, van Ooij P, Bandi K, et al. Viscous energy loss in the presence of abnormal aortic flow. Magn Reson Med 2014;72(3):620-628.

12. Itatani K, Sekine T, Yamagishi M, et al. Hemodynamic parameters for cardiovascular system in 4D flow MRI: Mathematical definition and clinical applications. Magn Reson Med Sci 2022;21(2):380-399.

13. Hayashi T, Itatani K, Inuzuka R, et al. Dissipative energy loss within the left ventricle detected by vector flow mapping in children: Normal values and effects of age and heart rate. J Cardiol 2015;66(5):403-410.

14. Honda T, Itatani K, Takanashi M, et al. Exploring energy loss by vector flow mapping in children with ventricular septal defect: Pathophysiologic significance. Int J Cardiol 2017;244:143-150.

15. Itatani K, Miyaji K, Tomoyasu T, et al. Optimal conduit size of the extracardiac Fontan operation based on energy loss and flow stagnation. Ann Thorac Surg 2009;88(2):565-572. discussion 72–3.

16. Itatani K, Okada T, Uejima T, Tanaka T, et al. Intraventricular flow velocity vector visualization based on the continuity equation and measurements of vorticity and wall shear stress. Jpn J Appl Phys 2013;52:07HF16.

17. Elbaz MSM, Scott MB, Barker AJ, et al. Four-dimensional virtual catheter: Noninvasive assessment of intra-aortic hemodynamics in bicuspid aortic valve disease. Radiology 2019;293(3):541-550.

18. Garcia J, Barker AJ, Markl M. The role of imaging of flow patterns by 4D flow MRI in aortic stenosis. JACC Cardiovasc Imaging 2019;12(2):252-266.

19. Markl M, Chan FP, Alley MT, et al. Time-resolved three-dimensional phase-contrast MRI. J Magn Reson Imaging 2003;17(4):499-506.

20. Takehara Y, Isoda H, Takahashi M, et al. Abnormal flow dynamics result in low wall shear stress and high oscillatory shear index in abdominal

aortic dilatation: Initial in vivo assessment with 4D-flow MRI. Magn Reson Med Sci 2020;19(3):235-246.

21. Wells RE, Merrill EW. Influence of flow properties of blood upon viscosity-hematocrit relationships. J Clin Invest 1962;41:1591-1598.

22. Bauernschmitt R, Schulz S, Schwarzhaupt A, et al. Simulation of arterial hemodynamics after partial prosthetic replacement of the aorta. Ann Thorac Surg 1999;67(3):676-682.

23. Sughimoto K, Takahara Y, Mogi K, et al. Blood flow dynamic improvement with aneurysm repair detected by a patient-specific model of multiple aortic aneurysms. Heart Vessels 2014;29(3):404-412.

24. Mathlouthi A, Locham S, Dakour-Aridi H, Black JH, Malas MB. Impact of suprarenal neck angulation on endovascular aneurysm repair outcomes. J Vasc Surg 2020;71(6):1900-1906.

25. Kelly R, Hayward C, Avolio A, O'Rourke M. Noninvasive determination of age-related changes in the human arterial pulse. Circulation 1989; 80(6):1652-1659.

26. Virmani R, Avolio AP, Mergner WJ, et al. Effect of aging on aortic morphology in populations with high and low prevalence of hypertension and atherosclerosis. Comparison between occidental and Chinese communities. Am J Pathol 1991;139(5):1119-1129.

27. Zhang C, Ohira M, Iizuka T, et al. Cardio-ankle vascular index relates to left ventricular ejection fraction in patients with heart failure: A retrospective study. Int Heart J 2013;54(4):216-221.

28. Vanagt WY, Famaey N, Rega F, Gewillig M. Extreme windkessel effect can cause right heart failure early after truncus repair. Interact Cardiovasc Thorac Surg 2012;15(1):181-182.

29. Tzilalis VD, Kamvysis D, Panagou P, et al. Increased pulse wave velocity and arterial hypertension in young patients with thoracic aortic endografts. Ann Vasc Surg 2012;26(4):462-467.

30. Takeda Y, Sakata Y, Ohtani T, et al. Endovascular aortic repair increases vascular stiffness and alters cardiac structure and function. Circ J 2014; 78(2):322-328.

31. Lee SC, Stevens TL, Sandberg SM, et al. The potential of brain natriuretic peptide as a biomarker for New York heart association class during the outpatient treatment of heart failure. J Card Fail 2002;8(3): 149-154.

32. Savarese G, Musella F, D'Amore C, et al. Changes of natriuretic peptides predict hospital admissions in patients with chronic heart failure: A meta-analysis. JACC Heart Fail 2014;2(2):148-158.

33. Tsutamoto T, Wada A, Maeda K, et al. Plasma brain natriuretic peptide level as a biochemical marker of morbidity and mortality in patients with asymptomatic or minimally symptomatic left ventricular dysfunction. Comparison with plasma angiotensin II and endothelin-1. Eur Heart J. 1999;20(24):1799-807.

34. Luchner A, Hengstenberg C, Lowel H, Riegger GA, Schunkert H, Holmer S. Effect of compensated renal dysfunction on approved heart failure markers: Direct comparison of brain natriuretic peptide (BNP) and N-terminal pro-BNP. Hypertension 2005;46(1):118-123.